



1 **Trifluoroacetic acid deposition from emissions of HFO-1234yf in India, China,**
2 **and the Middle East**

3

4 Liji M. David^{*1,2}, Mary Barth^{*3}, Lena Höglund-Isaksson⁴, Pallav Purohit⁴, Guus J. M. Velders^{5,6},
5 Sam Glaser^{1,7}, and Akkihebbal. R. Ravishankara^{*1,2}

6

7 ¹Department of Chemistry, Colorado State University, Fort Collins, CO 80523, USA

8 ²Department of Atmospheric Science, Colorado State University, Fort Collins, CO 80523, USA

9 ³Atmospheric Chemistry Observations and Modeling Laboratory, National Center for
10 Atmospheric Research, Boulder, Colorado

11 ⁴Air Quality and Greenhouse Gases Program, International Institute for Applied Systems Analysis
12 (IIASA), Schlossplatz 1, 2361, Laxenburg, Austria

13 ⁵National Institute for Public Health and the Environment (RIVM), PO Box 1, 3720 BA
14 Bilthoven, The Netherlands

15 ⁶Institute for Marine and Atmospheric Research Utrecht, Utrecht University, The Netherlands

16 ⁷Currently at Tufts University, Medford, MA

17

18 *Address correspondence to:* liji.david@colostate.edu, barthm@ucar.edu, and
19 a.r.ravishankara@colostate.edu

20

21 **Key points**

22 1. The expected concentrations of trifluoroacetic acid (TFA) from the degradation of HFO-
23 1234 yf (CF₃CF=CH₂) emitted now and in the future by India, China, and the Middle East
24 were calculated using GEOS-Chem and WRF-Chem models.

25 2. We conclude that, with the current knowledge of the effects of TFA on humans and
26 ecosystems, the projected emissions through 2040 would not be detrimental.

27 3. We carried out various tests and conclude that the model results are robust.

28 4. The major uncertainty in the knowledge of the TFA concentrations and their spatial
29 distributions is due to uncertainties in the future projected emissions.

30



31 **Abstract**

32 We have investigated trifluoroacetic acid (TFA) formation from emissions of HFO-1234yf, its dry
33 and wet deposition, and rainwater concentration over India, China, and the Middle East with
34 GEOS-Chem and WRF-Chem models. We estimated the TFA deposition and rainwater
35 concentrations between 2020 and 2040 for four previously published HFO-1234yf emission
36 scenarios to bound the possible levels of TFA. We evaluated the capability of GEOS-Chem to
37 capture the wet deposition process by comparing calculated sulfate in rainwater with observations.
38 Our calculated TFA amounts over the U.S., Europe, and China were comparable to those
39 previously reported when normalized to the same emission. A significant proportion of TFA was
40 found to be deposited outside the emission regions. The mean and the extremes of TFA rainwater
41 concentrations calculated for the four emission scenarios from GEOS-Chem and WRF-Chem were
42 orders of magnitude below the no observable effect concentration. The ecological and human
43 health impacts now and continued use of HFO-1234yf in India, China, and the Middle East are
44 estimated to be insignificant based on the current understanding, as summarized by Neale et al.
45 (2021).

46
47 **Keywords:** HFO-1234yf, Trifluoroacetic acid, wet and dry deposition, India, China, the Middle
48 East.

49
50 **1. Introduction**

51 The use of olefinic hydrofluorocarbons (HFCs) as substitutes for HFC-134a (1,1,1,2-
52 tetrafluoroethane, CF_3CFH_2) are increasing in both the developed and developing countries
53 (Velders et al., 2009). HFC-134a is a replacement for chlorofluorocarbons (CFCs) and
54 hydrochlorofluorocarbons (HCFCs), which were phased out under the Montreal Protocol and its
55 many amendments and adjustments (World Meteorological Organization, 2007). HFC-134a is a
56 potent greenhouse gas with a 100-year global warming potential (GWP) of 1300
57 (Intergovernmental Panel on Climate Change (IPCC) report (Myhre et al., 2013)). HFO-1234yf
58 (2,3,3,3-tetrafluoropropene, $\text{CF}_3\text{CF}=\text{CH}_2$) with a 100-year GWP of <1 (IPCC report (Myhre et al.,
59 2013)) is a replacement for HFC-134a in automobile air conditioners (MAC) (Papadimitriou et al.,
60 2008). The atmospheric degradation of HFO-1234yf leads to trifluoro acetyl fluoride ($\text{CF}_3\text{C}(\text{O})\text{F}$)
61 (Young and Mabury, 2010). $\text{CF}_3\text{C}(\text{O})\text{F}$ hydrolyzes rapidly to yield trifluoroacetic acid (TFA, $\text{CF}_3\text{-}$
62 $\text{C}(\text{O})\text{OH}$), which is removed from the atmosphere by dry and wet deposition (George et al., 1994).
63 The chemical lifetime of HFC-134a (~14 years) is such that it is reasonably well-mixed globally
64 upon emission into the atmosphere. Therefore, its degradation and the TFA formed will occur
65 across the globe. Only about 30% of the emitted HFC-134a leads to TFA (Kotamarthi et al., 1998).
66 A large fraction of the formed TFA is deposited into the oceans. The fraction of HFC-134a
67 degraded per year from one year's emission would be small, leading to small TFA in rainwater
68 concentrations at a given location. However, as HFC-134a accumulates in the atmosphere, more
69 TFA would be produced. HFO-1234yf has a shorter chemical lifetime of a few (~10) days (Myhre



70 et al., 2013) and its degradation leads almost exclusively (~100%) to $\text{CF}_3\text{C}(\text{O})\text{F}$. Therefore, TFA
71 deposition per year of emission will be higher, depend on the year, and more localized spatially.

72 Previous studies have focused on TFA formation from emissions of either HFC-134a at
73 the current or previous levels (Kanakidou et al., 1995; Kotamarthi et al., 1998) or HFO-1234yf
74 substituted for current levels of HFC-134a usage (Luecken et al., 2010); then, they have mostly
75 scaled it for scenarios of HFO-1234yf emissions in the future over the continental U.S. and Europe
76 (Henne et al., 2012; Papasavva et al., 2009). Some works have distinguished between uses of HFC-
77 134a in MAC versus total usage, while others have evaluated maximum use scenarios. These
78 studies suggest that toxic levels of TFA in water bodies are not produced over Europe, North
79 America, and China if HFO-1234yf replaces all the current use of HFC-134a (Henne et al., 2012;
80 Kazil et al., 2014; Luecken et al., 2010; Wang et al., 2018). Russell et al. (2012) conducted a model
81 study to determine TFA concentration in terminal water bodies in the contiguous U.S., with TFA
82 deposition rates from Luecken et al. (2010). They found that after 50 years of continuous
83 emissions, aquatic concentrations of 1 to 15 $\mu\text{g L}^{-1}$ are projected, with extreme concentrations of
84 up to 50 to 200 $\mu\text{g L}^{-1}$ in the arid southwestern U.S.

85 Kazil et al. (2014) investigated, using the WRF-Chem model, the atmospheric turnover
86 time of HFO-1234yf, the dry and wet deposition of TFA, and the TFA rainwater concentration
87 over the contiguous U.S. between May and September 2006. They also examined where TFA
88 deposited emissions of three specific regions in the U.S. They concluded that the average TFA
89 rainwater concentration was 0.89 $\mu\text{g L}^{-1}$ for the contiguous U.S. Although Kazil et al. (2014) used
90 emission twice as large as that used by Luecken et al. (2010), the TFA rainwater concentrations
91 were comparable. Kazil et al. (2014) used the measured HFC-134a to CO ratio from the Los
92 Angeles area to obtain potential HFO-1234yf emissions. They also showed that TFA rainwater
93 concentrations reached significantly higher values (7.8 $\mu\text{g L}^{-1}$) at locations with very low
94 precipitation on shorter time scales. A comparably low TFA wet deposition occurred in the dry
95 western U.S. The work of Wang et al. (2018) is similar to that of Henne et al. (2012) and used the
96 GEOS-Chem model and examined the rainwater content and deposited amounts of TFA over
97 Europe, the U.S, and China, with similar findings. Henne et al. (2012) is the only study that used
98 two different models (FLEXPART and STOCHEM) to study the TFA deposition and rainwater
99 concentration over Europe.

100 The above-noted studies focused on the U.S. and Europe, and most recently China. The
101 U.S. and Europe emissions of the sum of HFC-134a and HFO-1234yf are expected to increase
102 only in proportion to the population in the future since the per capita number of MAC, stationary
103 AC, and other cooling units are unlikely to increase rapidly. India, China, and the Middle East are
104 the regions with expected large increases in HFO-1234yf use. In these regions, the number of units
105 and associated usage will increase rapidly as the economies grow. Perhaps Latin America and parts
106 of Africa would also see similar increases. The above-noted studies from the U.S. and Europe do
107 not allow us to draw firm conclusions about TFA's formation from realistic future emissions from
108 Asia (China and the Indian subcontinent), where the markets are not saturated, and meteorology
109 is very different from North America and Europe. The rate of degradation of parent compounds



110 and precipitation will differ in the warmer tropical and subtropical regions from those seen for the
111 U.S. and Europe; the seasonality will also be different. The precipitation across Asia is associated
112 with the Asian monsoon, which is stronger in comparison to the monsoon in southwest U.S. It is
113 also essential to look at the Middle East emissions since the studies of Kazil et al. (2014) and
114 Russell et al. (2012) showed that TFA rainwater concentrations are larger over drier areas of the
115 U.S., and there can be more accumulation in arid regions.

116 In 2019 the Kigali Amendment to the Montreal Protocol went into force. According to the
117 amendment the production and use of HFCs has to be phased down in the coming decades. This
118 should reduce the emissions of HFCs such as HFC-134a, but will likely increase emissions of
119 HFO-1234yf.

120 A description of the models used (GEOS-Chem and WRF-Chem), HFO-1234yf emission
121 scenarios, and the chemical scheme are given in section 2. In section 3, we compare the
122 precipitation in GEOS-Chem and WRF-Chem with observations. We evaluate the GEOS-Chem
123 model's ability to reproduce wet deposition by comparing sulfate rainwater concentrations with
124 observations. We performed simulations using both the models for the three domains individually
125 to calculate the TFA's dry and wet deposition and rainwater concentrations over India, China, and
126 the Middle East. We performed two-year runs in GEOS-Chem to check for interannual variability.
127 We compare our simulation results with other studies for the U.S., Europe, and China. The HFO-
128 1234yf emissions from all the regions together were also simulated to assess the interregional
129 effects. Major findings from this study are summarized in section 4.

130

131 2. Methods

132 2.1. Model description

133 **GEOS-Chem:** We used the GEOS-Chem (v12.0.3, www.geos-chem.org) global three-
134 dimensional chemical transport model driven by GEOS-FP assimilated meteorological data.
135 GEOS-Chem has a fully coupled tropospheric NO_x-O_x-hydrocarbon-aerosol chemistry. The
136 simulations were made at 2°×2.5° resolution and 47 vertical levels from the surface to ~80 km.
137 The wet deposition of aerosols and soluble gases by precipitation includes the scavenging in
138 convective updrafts, in-cloud rainout, and below-cloud washout (Amos et al., 2012; Liu et al.,
139 2001). The dry deposition was calculated using a resistance-in-series parameterization, which is
140 dependent on environmental variables and lookup table values (Wesely, 1989). The simulations
141 were conducted for 2015 and 2016 following a 2-month spin-up.

142 The global anthropogenic emissions were from Emissions Database for Global
143 Atmospheric Research (version 4.3). The global emissions are superseded by regional emission
144 inventories for India (Speciated Multi-pollutants Generator (SMOG) and MIX) (Li et al., 2017;
145 Pandey et al., 2014; Sadavarte and Venkataraman, 2014), China (MIX), Europe (EMEP), U.S.
146 (National Emissions Inventory (NEI) 2011) (NEI2011, [http://www.epa.gov/air-emissions-](http://www.epa.gov/air-emissions-inventories)
147 [inventories](http://www.epa.gov/air-emissions-inventories)), Canada (Criteria Air Contaminants (CAC), <http://www.ec.gc.ca/>), and Mexico
148 (BRAVO) (Kuhns et al., 2005). We used the biomass burning from Global Fire Emissions
149 Database (GFED) version 4 (Giglio et al., 2013). The biogenic VOC emissions were from the



150 Model of Emissions of Gases and Aerosols from Nature (MEGAN) version 2.1 inventory of
151 Guenther et al (2012). The details on other emissions are described in David et al. (2018, 2019).

152 **WRF-Chem:** The Weather Research and Forecast with Chemistry (WRF-Chem) model (Fast et
153 al., 2006; Grell et al., 2005) version 4.1.3, was used to simulate meteorology and chemistry over
154 India, China, and the Middle East individually. The WRF-Chem simulations were integrated for
155 14 months, beginning 1 November 2014 and ending 31 December 2015, with the first two months
156 of the simulation was used to spin up the model chemistry. The three model domains, shown in
157 Figure 1, have a horizontal grid spacing of 30 km and 40 vertical levels reaching a model top of
158 50 hPa. The vertical levels stretch in size with a fine resolution near the surface and a coarser
159 resolution in the upper troposphere. The model meteorology was initialized with Global Forecast
160 System (GFS) archived at 0.5° and a temporal resolution of 6 hours. Observational nudging is
161 applied for temperature, moisture, and winds to keep large-scale features in line with the observed
162 meteorology. The model physics and chemistry options that were used are summarized in Table
163 S1 in the supplementary information. The Model for Ozone and Related chemical Tracers
164 (MOZART) gas-phase chemical mechanism and the Global Ozone Chemistry Aerosol Radiation
165 and Transport (GOCART) scheme for aerosols (MOZCART) (Pfister et al., 2011) were used to
166 simulate ozone and aerosol chemistry. TFA chemistry was added to this chemical option. Six-
167 hourly results from the Community Atmosphere Model with Chemistry (CAM-Chem), which has
168 a similar chemistry mechanism as the WRF-Chem model configuration, were used (Tilmes et al.,
169 2015) to initialize trace gas and aerosol mixing ratios as well as to provide lateral boundary
170 conditions. HFO-1234yf and TFA were initialized with the GEOS-Chem results described above.
171 The Model of Emissions of Gases and Aerosols from Nature (MEGAN v2.04; Guenther, 2007)
172 was used to represent the net biogenic emissions for both gases and aerosols. Anthropogenic
173 emissions were from the Emissions Database for Global Atmospheric Research – Hemispheric
174 Transport of Air Pollution (EDGAR-HTAP) emission inventory (Janssens-Maenhout et al., 2015).
175 The Fire Inventory from NCAR version 1 (FINNv1.6; Wiedinmyer et al., 2011) was implemented
176 to provide daily varying emissions of trace species from biomass burning.

177 The wet removal scheme in WRF-Chem for MOZART chemistry, based on Neu and
178 Prather (2012), was used to compute the dissolution of soluble trace gases into precipitation and
179 their release into the gas phase upon evaporation of hydrometeors. Neu and Prather (2012) estimate
180 trace gas removal by multiplying the effective Henry's law equilibrium aqueous concentration by
181 the net precipitation formation (conversion of cloud water to precipitation, minus evaporation of
182 precipitation). Dry deposition of trace gases was described with the Wesely (1989)
183 parameterization. Diagnostic information on the wet and dry deposition of TFA was determined
184 every time step and accumulated values were included in the output files.

185

186 2.2. Emissions

187 HFO-1234yf is just now entering the market driven by regional (e.g., the European Union's
188 MAC Directive 2006/40/EC), national (e.g., Japan and U.S.) F-gas regulations, and the Kigali
189 Amendment to the Montreal Protocol. HFC-134a is currently the primary working fluid of MAC



190 and other applications (refrigerant, insulating foams, and aerosol propellants). Therefore, we have
191 to estimate the future emission levels from the three regions of interest. Unlike the developed
192 countries, India, China, and the Middle East are growing rapidly and the use of air conditioning
193 and refrigeration (and other uses of HFCs and HFOs) are expected to increase rapidly. Therefore,
194 one has to consider the likely economic growth and other factors in estimating emissions levels.
195 Here, we explore a few different potential scenarios for emissions of HFO-1234yf.

196 TFA production from HFO-1234yf increases linearly with the rise in HFO-1234yf
197 emissions, i.e., there is no feedback on this process since the primary drivers for the degradation
198 of this chemical, the OH radical, will not be altered by their relatively small emissions. In addition,
199 the changes in the abundance of OH in the troposphere in the next few decades are unlikely to be
200 different (say <13%) than the current levels based on the changes seen over the past few decades
201 (Rigby et al., 2017). Therefore, we can estimate the extent of TFA formation from a set of
202 modeling calculations that employed a fixed total amount of HFO-1234yf from each region. After
203 that, we can calculate the extent of TFA formation for various possible emission scenarios.

204 We used four future HFO-1234yf emissions scenarios for the 2020 to 2040 period: (1)
205 estimate of the upper range scenario HFO-1234yf emissions based on Velders et al. (2015)
206 estimate; (2) lower range scenario of HFO-1234yf based on Velders et al. (2015) estimate; (3) the
207 Greenhouse Gas Air Pollution Interactions and Synergies (GAINS) model (Amann et al., 2011)
208 with maximum technically feasible reduction (MTFR) estimates of HFO-1234yf; and (4) the
209 GAINS ‘maximum HFO’ (max HFO) scenario. Given the relatively short lifetime of HFO-1234yf,
210 the TFA production per year is dependent only on the emissions in that year. Figure 2 shows the
211 HFO-1234yf emission projection from India, China, and the Middle East for the four scenarios
212 between 2020 and 2040. The scenario based on Kumar et al. (2018) is similar to the fourth scenario
213 we considered. Therefore, we have not specifically included this possibility.

214 The emission estimates of HFO-1234yf in the GAINS model depends on when countries
215 will comply with the Kigali Amendment, current and future emissions based on country-level
216 activity data, uncontrolled emission factors, the removal efficiency of emission control measures,
217 and the extent to which such measures are applied (Purohit and Höglund-Isaksson, 2017). The
218 GAINS model uses the fuel input for the transport sector that is provided by the exogenous
219 projections (e.g., International Energy Agency’s World Energy Outlook 2017). First, using the
220 annual mileage per vehicle (veh-km) and specific fuel consumption (SFC), GAINS estimates the
221 number of vehicles (by type, fuel). Second, using the penetration rate of a MAC, the number of
222 vehicles with MAC is calculated. Next, using the specific refrigerant charge (different for MAC
223 used in vehicle types), the HFO-1234yf consumption in mobile air conditioners is calculated. Note
224 that the HFO-1234yf is assumed to be substituted for HFC-134a, one-to-one, in all vehicles. For
225 HFO-1234yf use in MAC, HFO-1234yf emissions are estimated separately for “banked”
226 emissions, i.e., leakage from equipment in use, and for “scrapping” emissions, i.e., emissions
227 released at the end-of-life of the equipment. The leakage rate in the GAINS model assumes a
228 percentage of the charge per year. For example, if the refrigerant charge in MAC is 0.5 kg then the
229 emissions from the bank will be 0.05 kg (= 0.5 kg×0.1) per year, where the leakage rate is 10%



230 per year. This leakage rate is a steady refrigerant loss through seals, hoses, connections, valves,
231 etc. from every MAC over the entire use-phase (annually). At the end-of-life, the scrapped
232 equipment is assumed to be fully loaded with refrigerant, which needs recovery, recycling, or
233 destruction. At the same time, if there are regulations in place (e.g., MAC Directive 2006/40/EC
234 in European Union) - a package of measures including leak prevention during use and refill,
235 maintenance, and end of life recovery, and recollection of refrigerants, GAINS consider these good
236 practices as a control option with a removal efficiency of 50% for *in-use* and 80% for *end-of-life* -
237 based on secondary sources (Purohit et al., 2020). However, no such measures are assumed for
238 India, China, and the Middle East. Thus, these emissions can be considered the maximum likely
239 emissions. The MTRF version of the GAINS scenario assumes that the maximum technically
240 feasible reductions are applied across the sectors in India, China, and the Middle East. The Velders
241 et al. (2015) emissions also follow the Kigali amendment. The ‘Shared Socioeconomic Pathways’
242 (SSPs) SSP3 and SSP5 are the lower and upper range scenarios, respectively, used in Velders et
243 al. (2015) calculated for 11 geographic regions and 13 use categories. Kumar et al. (2018) highlight
244 that many applications in India will likely transition to something other than HFOs. These trends
245 are not unique to India and will likely be replicated in China and the Middle East. Therefore, the
246 four HFO-1234yf emission scenarios for the 2020 to 2040 period represent emissions that are
247 higher than should be expected and, therefore, are upper limit estimates of the potential impact of
248 TFA in these regions.

249 To minimize numerical errors (in using small emissions) and compare them with previous
250 studies, we used HFO-1234yf emissions of ~ 40 Gg yr⁻¹ from each of these regions. This value
251 corresponds to 2025 projected emissions from the GAINS model over India and the Middle East
252 if all the applications were to use HFO-1234yf in place of HFC-134a for China, the emission values
253 are for 2016 from Wang et al. (2018). Figure S1 in the supplementary information shows the annual
254 spatial distribution of HFO-1234yf over India, China, and the Middle East as simulated in: (i)
255 GEOS-Chem; and (ii) WRF-Chem models. We distributed this total emission across the
256 country/region of interest by scaling the emission to known anthropogenic CO emissions used in
257 the model. The anthropogenic CO is a good tracer for HFO-1234yf emissions since they originate
258 from similar applications (especially the transport sector) and in proportion to the distribution of
259 economic activities in the region/country of interest. We show the total emissions in each of the
260 three regions in both the models in the figure. The distribution varies to a small extent with the
261 season (shown in Figure S2 in the supplementary information), and the monthly variation in
262 emission is similar in both models. We also simulated GEOS-Chem over the US and Europe using
263 the total HFO-1234yf emissions from Wang et al. (2018) and Henne et al. (2012), respectively.

264

265 **2.3. Chemical scheme**

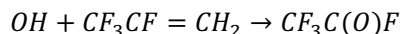
266 The chemical degradation of HFO-1234yf and the production of TFA were added to both
267 the GEOS-Chem NO_x-O_x-hydrocarbon-aerosol chemistry scheme and the WRF-Chem
268 MOZCART chemistry scheme. The detailed chemical scheme for the formation of TFA from



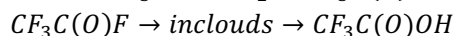
269 HFO-1234yf is shown in Burkholder et al. (2015) and, therefore, not repeated here. The simplified
270 representation of TFA production follows that of Kazil et al. (2014):

271

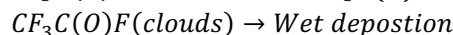
272



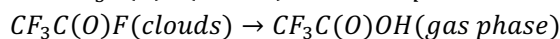
273



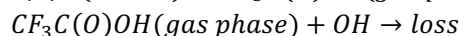
274



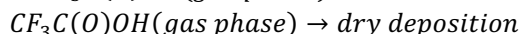
275



276



277



278

279

280

281

282

283

284

285

286

287

288

289

290

291

292

293

294

295

296

297

298

299

300

301

302

303

304

305

306

307

308

3. Results and Discussion

3.1. Sulfate concentration in rainwater

Wet deposition is one of the primary removal processes for TFA. This deposition depends on precipitation amounts and how well our model captures the wet deposition process, making it crucial to evaluate the models used here to capture these two factors.

First, we compared the annual total precipitation amounts calculated by GEOS-Chem and WRF-Chem with the observed daily total accumulated precipitation from the Tropical Rainfall Monitoring Mission (TRMM_3B42_daily product) in the three regions (Figure S3a in the supplementary information). The TRMM product is at a $0.25^\circ \times 0.25^\circ$ resolution. The spatial distribution of seasonal total precipitation in the three domains from the two models and TRMM is shown in Figure S4 in the supplementary information. Both the models captured the seasonal



309 precipitation patterns. As seen in Figure S3a, the total precipitation amounts were a factor of 1.5-
310 2 higher in GEOS-Chem compared to WRF and TRMM. (The ratio of total precipitation between
311 GEOS-Chem and WRF-Chem(TRMM) were 2.6 (1.5), 2.2 (1.5), and 2.2 (1.4) for India, China,
312 and the Middle East, respectively). WRF-Chem underestimated the precipitation amounts
313 compared to TRMM in the three regions. Kumar et al. (2012; 2018) have addressed the
314 precipitation biases in WRF-Chem compared to TRMM over South Asia. We attribute the higher
315 precipitation in GEOS-Chem to: (a) the different model physics used; (b) the effects of a
316 meteorology-driven chemistry transport model (GEOS-Chem) versus an “online” chemistry
317 transport model (WRF-Chem) where chemistry is solved at the same time step as the meteorology;
318 (c) and to the different grid spacings used by the two models, noting that the coarse GEOS-Chem
319 grid cells contain several convective storms compared to that in WRF-Chem. The monthly
320 variation in total precipitation is shown in Figure S3b (supplementary information), and both
321 models have similar trends as that observed by TRMM.

322 To evaluate the accuracy of the TFA wet deposition, it is useful to compare sulfate wet
323 deposition amounts produced by the oxidation of SO₂. The emissions of SO₂ are comparable in
324 both the models (shown in Figure S5 in the supplementary information). We have measurements
325 of sulfate rainwater concentrations in some of the regions. Further, the lifetime of SO₂ in the
326 troposphere is comparable to that of HFO-1234yf. We hasten to add that while the HFO-1234yf
327 degradation is controlled by gas phase OH reactions, that of SO₂ include both gas and condensed
328 phase processes. However, the removal of both sulfate and TFA are due to condensed phase
329 reactions. The WRF-Chem model has been shown to capture the sulfate rainwater concentration
330 over the continental U.S. by Kazil et al. (2014); we expect it to do well over this study's regions.
331 However, GEOS-Chem has not been evaluated previously. There are no networks for measuring
332 sulfate rainwater concentration in India and the Middle East. Yet, there are some observations of
333 rainwater sulfate in the published articles in all three domains. The available data are sparse, and
334 the observations for 2015 (the modeled year) are even fewer to make a comparison with WRF-
335 Chem simulations. However, GEOS-Chem simulations were available from our previous work for
336 2000-2015. We used those results to compare with observations during that period. The
337 observation locations (over land only) in the three domains are shown in Figure S6 in the
338 supplementary information. Figure 3 shows the scatter plot of simulated and observed sulfate
339 rainwater concentration in the three domains. Table 1 lists the statistics of the comparison between
340 GEOS-Chem and the observations. Rainwater sulfate amounts calculated by GEOS-Chem
341 correlate well ($R > 0.80$) with observations. We see a bias of -13, -13, and -3% in India, China, and
342 the Middle East domains, respectively. The negative bias in GEOS-Chem sulfate rainwater
343 concentration could be because the model integrates over a large area while the observations are
344 point locations. It could also be, as noted earlier, because GEOS-Chem yields higher amounts of
345 precipitation and thus could lead to smaller rainwater concentrations. We suggest that these values
346 are good to at least a factor of two. In summary, the GEOS-Chem model shows considerable skill
347 in reproducing mean sulfate rainwater concentrations and spatial variability of sulfate rainwater
348 concentrations; therefore, it can be utilized to calculate TFA wet deposition.



349

3.2. Comparison of calculated TFA with previous studies

351 Before presenting the results of the calculations for India, China, and the Middle East from
352 the present study, we note that our models agree with the previous studies over the U.S. (Kazil et
353 al., 2014; Luecken et al., 2010), China (Wang et al., 2018), and Europe (Henne et al., 2012). Figure
354 4 shows the comparison of annual mean (a) TFA deposition (dry and wet combined), and (b) TFA
355 rainwater concentration over the U.S., China, and Europe. We have normalized the emissions to
356 match those of the previous studies for meaningful comparisons. (The emissions used to compare
357 TFA from the U.S., China, and Europe are 24.5, 42.7, and 19.2 Gg yr⁻¹, respectively.) We note that
358 average deposition rates differ in the model because of the differences in calculations' domain
359 sizes. Given that the models vary in their versions, meteorology, physics, and the expected model
360 variabilities, the observed agreement is reasonable. We also show the comparison with our
361 calculations over the U.S. for the summer months with previous studies (Kazil et al., 2014;
362 Luecken et al., 2010; Wang et al., 2018) (Figure S7 in the supplementary information).

363

3.3. Atmospheric mixing ratios

365 Figure 5 shows the annual mean mixing ratios of HFO-1234yf over India, China, and the
366 Middle East as simulated by GEOS-Chem and WRF-Chem. We present here only results with
367 emissions in GEOS-Chem(WRF-Chem) of 41.3(41.9), 40.6(39.9), and 37.8(38.1) Gg yr⁻¹ from
368 India, China, and the Middle East, respectively. Expected TFA for other emissions can be simply
369 scaled to the emissions of interest. The annual mean mixing ratio of HFO-1234yf in India, China,
370 and the Middle East as simulated by GEOS-Chem(WRF-Chem) were 2.87(3.94) ppt, 2.49(3.70)
371 ppt, and 1.82(2.49) ppt, respectively, and below 1 ppt (as seen in GEOS-Chem) outside of the three
372 regions. The annual mean mixing ratio in the China domain was comparable to Wang et al. (2018).
373 The highest (>40 ppt) simulated annual mean HFO-1234yf mixing ratio for India was in the Indo-
374 Gangetic Plain (IGP), for China in the northeast region, and for the Middle East in northern Iran.
375 The emission hotspots (Figure S1 in the supplementary information) in the three regions led to the
376 largest annual mean HFO-1234yf mixing ratios in those regions. The WRF-Chem simulated higher
377 annual mean HFO-1234yf mixing ratios compared to GEOS-Chem. Differences in annual mean
378 HFO-1234yf mixing ratios between models for the same amount of emissions have been reported
379 also by Henne et al. (2012). However, the overall spatial patterns are comparable between GEOS-
380 Chem and WRF-Chem. It should be noted that the change of HFO-1234yf emissions in any of the
381 three regions would change the HFO-1234yf mixing ratio within that region and will have minimal
382 effect on other regions.

383

3.4. TFA deposition

385 GEOS-Chem simulated mean total deposition rates (dry and wet deposition combined) to
386 be 0.874, 0.501, and 0.477 kg km⁻² yr⁻¹, respectively, in India, China, and the Middle East domains
387 for emissions of 41.3, 40.6, and 37.8 Gg yr⁻¹, respectively. WRF-Chem simulated mean deposition
388 rates (dry and wet) were 0.802, 0.342, and 0.284 kg km⁻² yr⁻¹ in India, China, and the Middle East



389 domains, respectively (Figure S8 in the supplementary information). Figure 6 shows the annual
390 total dry and wet TFA deposition rates in the three domains. The total annual dry deposition in
391 GEOS-Chem and WRF-Chem over the India domain was largest in eastern India and Bangladesh,
392 reaching up to $2 \text{ kg km}^{-2} \text{ yr}^{-1}$. The wet deposition in the India domain mostly occurred in the
393 Himalayas' foothills, eastern IGP, parts of central India, and southwest India and was $>3.5 \text{ kg km}^2$
394 yr^{-1} . In the China domain, the total dry and wet deposition rates in GEOS-Chem and WRF-Chem
395 were highest in southeast China. The total dry deposition rate in the Middle East domain was
396 highest in northern Iran. The wet deposition rate was the largest in parts of Iran, with differences
397 between the models. The wet deposition dominated the total TFA deposition. The combined annual
398 total deposition pattern was similar to that of wet deposition in the three domains (Figures 6 and
399 S8 in the supplementary information). The seasonal total deposition rates of TFA from dry and
400 wet depositions in the three domains are shown in Figure S9 in the supplementary information.
401 The seasonal deposition rates were highest for June-September, June-August, and April-October
402 in India, China, and the Middle East domains, respectively.

403 Figure 7 shows the percentage contribution of dry and wet deposition to total TFA
404 deposition between GEOS-Chem and WRF-Chem in the three domains. It should be noted that the
405 sum of the two (dry and wet) percent contribution do not add up to exactly 100% because of
406 transport in and/or out of the domains. For the total amount of HFO-1234yf emissions mentioned
407 in Figure S1 (supplementary information) and discussed in section 2.2, the total TFA deposition
408 (dry and wet combined) in India, China, and the Middle East domains from GEOS-Chem were
409 23.4, 20.5, and 18.7 Gg yr^{-1} , respectively. The total annual dry(wet) deposition amounts account
410 for 21(36)%, 20(31)%, and 20(29)% of the annual emissions of HFO-1234yf in GEOS-Chem. In
411 WRF-Chem, annual total TFA deposition was 19.4, 12.1, and 9.9 Gg yr^{-1} , respectively, in India,
412 China, and the Middle East domains. The dry(wet) TFA deposition was 10(37)%, 3(23)%, and
413 4(26)% of the emissions in India, China, and the Middle East domains, respectively. Table S2
414 (Supplementary Information) shows the seasonal TFA deposition (dry and wet) calculated from
415 GEOS-Chem and WRF-Chem models in the three domains. The lower TFA deposition in WRF-
416 Chem compared to GEOS-Chem is due to the venting of surface emissions into the free
417 troposphere (Grell et al., 2004; Kazil et al., 2014) that leads to lower dry deposition in WRF-Chem
418 (Figure 7a). The differences in deposition between models can also be attributed to differences in
419 model resolutions, model transport, meteorological conditions (e.g., precipitation), and cloud
420 treatment. These differences highlight the need for multi-model simulations to estimate the likely
421 variation in these parameters.

422 Figure 8 shows the total TFA deposition (dry and wet combined) for the four emission
423 scenarios (Figure 2) calculated from GEOS-Chem and WRF-Chem. Our results show that the
424 differences in the calculated extent of TFA formed and deposited are about a factor of two between
425 the models. In all cases, the computed TFA dry and wet deposition varies linearly with the
426 emissions. Therefore, we can calculate the amounts of TFA formed and deposited for any
427 envisioned emission of HFO-1234yf.

428



429 3.5. Rainwater concentrations

430 Figure 9 shows the monthly variation in mean TFA rainwater concentration in the three
431 domains calculated from GEOS-Chem and WRF-Chem. The TFA rainwater concentration also
432 varies linearly with the emissions. Figure 9 shows the following: (a) higher concentrations are to
433 be expected when there is little rain/precipitation (Figure S3b in the supplementary information)
434 to remove TFA. This point has been noted in previous studies (Kazil et al., 2014; Russell et al.,
435 2012; Wang et al., 2018). So, if all the TFA were concentrated into a small amount of rain, the
436 concentrations have to be larger. Such events are infrequent. They are, relative to the rainier
437 regions, more frequent in the Middle East. The large rainwater concentration does not mean that
438 the amount of deposited TFA is larger; (b) The rainwater concentrations varied inversely with the
439 precipitation amount, as seen by comparing the rainwater TFA levels with the total precipitation
440 (Figure S3 in the supplementary information). A clear signal for the rainfall variation was seen
441 over India, where the monsoon season (June, July, August, and a part of September) bring large
442 and almost constant precipitation. This large precipitation makes the TFA rainwater concentrations
443 extremely small. In other words, this is simply a dilution effect; (c) When the rainfall is small,
444 there are considerable variations as one would expect. Lesser total precipitation arises because of
445 fewer showers and often in spatially and temporally sporadic events. So, the concentrations can
446 vary a great deal. This was also evident over China during dry seasons; and (d) the calculated TFA
447 rainwater concentrations were comparable to previous calculations for China (scaled to emissions,
448 Figure 4b).

449 It is important to know the regions of high TFA rainwater concentrations. Therefore, we
450 plotted the spatial pattern of annual mean TFA rainwater concentration in the three domains from
451 both models (Figure S10 in the supplementary information). It is noticeable that most of the regions
452 in all three domains did not have high TFA rainwater concentrations. There were some grids with
453 TFA rainwater concentrations that exceeded $50 \mu\text{g L}^{-1}$ for emissions of $\sim 40 \text{ Gg yr}^{-1}$. The high TFA
454 rainwater concentration seen in the western part of India and China domains is because of input at
455 the lateral boundaries from a global model. As mentioned in section 3.1, the precipitation in GEOS-
456 Chem was higher, resulting in lower TFA rainwater concentration. Focusing on the highest
457 possible rainwater concentrations is misleading since that does not tell us the amount of wet TFA
458 deposition, which is shown in Figure 6. However, it is clear that if the emissions of HFO-1234yf
459 reach the large numbers noted by the IIASA/GAINS model (max HFO, Figure 2d) for 2040, there
460 will be significant areas with larger TFA rainwater concentrations. The wet deposition does not
461 tell the whole story either since a substantial fraction of the rainwater ends up in the oceans every
462 year. The estimation of the TFA retained on land will be critical for further estimating the long-
463 term impact. Such a hydrology study is warranted but beyond the scope of this work.

464 3.5.1. Comparison of expected TFA rainwater levels with No Observable Effects 465 Concentrations

466 The primary reason for carrying out these calculations was to estimate the potential impact
467 of HFO-1234yf usage in the three regions of the study for the current and future emissions. The
468 effects of interest here are TFA formation from HFO-1234yf and its consequences to human and



469 ecosystem health. Figure 10 shows the mean TFA rainwater concentration for the four emission
470 scenarios calculated from GEOS-Chem and WRF-Chem. In all the scenarios, the annual mean
471 TFA rainwater concentration was well below the no observed effect concentration (NOEC) for
472 aquatic species, which is $>10,000 \mu\text{g L}^{-1}$ (Solomon et al., 2016), with an outlier for the most
473 sensitive alga as $120 \mu\text{g L}^{-1}$ (Boutonnet et al., 2011).

474 Neale et al. (2021) have summarized the impact of TFA on human and ecosystem health.
475 Their conclusion suggests that the NOEC on aquatic systems is $>10,000 \mu\text{g L}^{-1}$. As shown in
476 Figures 9, 10, and S10 (supplementary information), the expected rainwater concentrations are at
477 least two orders of magnitude lower than the NOEC. Also, the rainwater concentrations of TFA,
478 even for the 2040 emissions, are roughly comparable to those currently observed in China (Chen
479 et al., 2019) and about ten times greater than those presently observed over Germany (Freeling et
480 al., 2020). They also note that large TFA concentrations have been observed in people's blood in
481 China with no ill effects on the endpoints measured in that work (Duan et al., 2020).

482 TFA quantities deposited via dry deposition to land and vegetation would be much smaller
483 than those noted in Neale et al. (2021) to have any significant detrimental health effect. Indeed,
484 they note that there are other sources of TFA that are much higher than those expected from HFO-
485 1234yf degradation. Neale et al. (2021) also point out that the TFA deposited to snow in the Arctic
486 would not significantly contribute to marine water bodies even if it all melted down since the
487 volume of the melt would be much smaller than those of the receiving water bodies.

488 Lastly, since TFA can accumulate over land and water bodies, we can estimate the
489 influence of accumulation on the potential future impacts. The total TFA amount in rainfall would
490 not change. However, the amounts in water bodies could increase. For the 20 years modeled here,
491 the total TFA in water bodies would be larger than those observed for 2020 if TFA merely
492 accumulates. It is hard to calculate precisely where the water bodies would accumulate TFA
493 without a hydrological model. However, these values would still be orders of magnitude smaller
494 than the NOEC of $>10,000 \mu\text{g L}^{-1}$. For example, if all the TFA produced in these regions were to
495 end up in the top 15 meters of the world's oceans, we expect the TFA levels to increase by about
496 $0.015 \mu\text{g L}^{-1}$ by 2040.

497 Based on these observations, and assuming that the NOEC concentration holds, it appears
498 that the TFA from the expected emissions of HFO-1234yf in these three regions would not
499 constitute a health threat to plants or humans (even if we assume that there is no water treatment
500 to remove TFA in drinking water).

501

502 3.6. Interannual variability

503 The model results discussed in the previous sections are for one year, 2015. To assess the
504 influence of interannual variability in meteorology, we simulated the TFA deposition and
505 rainwater concentration for 2016 with the GEOS-Chem model for the total HFO-1234yf emissions
506 described in section 2.2. Figure 11 shows the fraction of TFA in the three domains for 2015 and
507 2016 that is: (a) dry deposited; (b) wet deposited; and (c) the annual mean TFA rainwater
508 concentrations. The total precipitation in both years was comparable (shown in Figure S11 in the



509 supplementary information). The results of our two-year simulations lead us to conclude that the
510 interannual differences are small. Therefore, we suggest that the results of 2015 are applicable
511 going forward to 2040.

512

513 **3.7. Simultaneous emissions from multiple regions**

514 It is important to note that most TFA is deposited outside of the domains, even though the
515 estimated lifetime of HFO-1234yf is about ten days. Therefore, TFA is dispersed significantly
516 from the source region. Figure 12a shows that roughly 25-50% of the HFO-1234yf emitted from
517 a given region was converted and deposited (via dry and wet deposition) as TFA within the domain
518 (see Figure 1 for domain boundaries). Figure 12b shows the percentage of TFA deposition (dry
519 and wet combined) calculated from GEOS-Chem and WRF-Chem within the three domains over
520 land. The remaining TFA was transported outside the domain. It is difficult to quantify the exact
521 locations of these depositions outside the domain since the concentrations get very small even
522 though in the aggregate that accounts for somewhere between 30% and 45%. The fraction that was
523 deposited within the region of emission was even smaller and ranged between 7% and 27%.
524 Therefore, it can be concluded that a significant fraction ended up in the oceans. This is especially
525 true for India and the Middle East emissions. Interestingly, a substantial amount of the TFA from
526 the Middle East emissions deposited in the Arabian Sea. Therefore, we conclude that even though
527 HFO-1234yf is short-lived, it is still sufficiently long-lived to travel thousands of kilometers. Such
528 an expectation is in accord with the calculated distances traveled by an air mass for even about 2
529 m s^{-1} .

530 The deposition outside of the region and domains also means that the emitting regions are
531 not the only area affected by their emission of HFO-1234yf. This is in spite of the relatively short
532 turnover time of HFO-1234yf. (Note: We call this the turnover time since because of the way we
533 calculate it in the model.) Since the three countries/regions studied here are adjacent to each other
534 and their domains overlap (Figure 1), it is possible to estimate the impact of the neighbors'
535 emission on each other. We consider the emissions over the rest of the world (excluding India,
536 China, the Middle East, the US, and Europe) from Fortems-Cheiney et al. (2015) assuming HFC-
537 134a is substituted with HFO-1234yf on a mole-per-mole basis (the maximum likely emissions
538 scenario). Figure S12 in the supplementary information shows the annual spatial distribution of
539 HFO-1234yf emissions from all the regions as simulated in GEOS-Chem. The percentage
540 deposition of TFA (dry and wet combined) from global and regional (individual regions) emissions
541 of HFO-1234yf is shown in Figure 13. The TFA deposition increased by 7-18% in the three
542 domains because of the emissions from its neighbors. Figure 13 suggests that if the entire world
543 switches to HFO-1234yf, the impact of TFA from the near and far neighbors would be noticeable,
544 but still be at most a factor of 2 or 3 larger. Figure S13 in the supplementary information shows
545 the spatial pattern of the annual total TFA via (a) dry and (b) wet deposition rates from global
546 emissions of HFO-1234yf. The dominant TFA deposition regions were most parts of India,
547 southeast China, parts of Iran, and the southern Arabian Sea. We discussed in section 3.5.1 the
548 potential impacts of such a global switch.



549

550 3.8. Reaction of TFA with Criegee intermediates

551 We examined the influence of CI's potential reactions with TFA on its tropospheric levels.
552 We used the CI concentrations in the boundary layer (0-2 km) from Chhantyal-Pun et al. (2017)
553 in GEOS-Chem and simulated the model for seven months (January to July) using 2015
554 meteorology. Figure S14 in the supplementary information shows the mean surface CI
555 concentration for those seven months calculated at $2^\circ \times 2.5^\circ$ spatial resolution. The CI
556 concentrations in the three regions of our study were less than $2500 \text{ molecules cm}^{-3}$. We calculated
557 the percentage decrease in total TFA deposition within the three domains by including the CI
558 chemistry. We assumed at all the CI reactions with TFA have the rate coefficient measured for
559 that of CH_2OO with TFA, i.e., $5 \times 10^{-18} T^2 e^{1620/T} \text{ cm}^3 \text{ molecules}^{-1} \text{ s}^{-1}$. Figure 14 shows the
560 spatial pattern of decrease in total TFA deposition (dry and wet combined) for seven months. In
561 most of the locations within the three domains, the decrease in total TFA deposition was $<2.5\%$.
562 At a few places in southeast Asia (Figure 14a), western China (Figure 14b), and northern Africa
563 (Figure 14c), the TFA deposition decreased by 7-25%. The decrease in TFA deposition due to CI
564 was 0.03, 0.32, and 0.08 Gg (total for seven months) for India, China, and the Middle East
565 domains, respectively. Overall, the impact of CI on TFA deposition was small in the region of
566 study.

567

568 4. Summary

569 We have investigated TFA formation from emissions of HFO-1234yf, its dry and wet
570 deposition, and rainwater concentration over India, China, and the Middle East with GEOS-Chem
571 and WRF-Chem models. We estimated the TFA deposition and rainwater concentrations between
572 2020 and 2040 for four HFO-1234yf emission scenarios. The models were simulated for a year
573 (2015), with additional 2016 simulations to understand the interannual variability. We also
574 simulated the model using global emissions to assess interregional effects on TFA deposition. The
575 main results of the study are summarized below:

- 576 • Using two models at different spatial resolutions helped us assess the variation in model
577 transport, precipitation, and cloud treatment. These variations yield slightly different
578 calculated TFA levels from the emission of HFO-1234yf. Even though there are discernable
579 differences, the overall conclusions are the same and point to this study's robustness.
- 580 • The accuracy of the GEOS-Chem model's ability to calculate wet deposition over the regions
581 of interest was tested by comparing calculated sulfate rainwater concentration with
582 observations. The model reproduces well the multiyear sulfate rainwater concentration (-3%
583 to -13% bias) and its spatial variability ($R > 0.80$) in the three domains.
- 584 • Our calculated TFA amounts over the U.S., Europe, and China were comparable to those
585 previously reported when normalized to the same emissions.
- 586 • The controlling factor for the amount of TFA from HFO-1234yf is its emissions. The
587 uncertainties in the models and chemistry are secondary to the extent of emissions.



- 588 • The TFA deposition was largest over eastern India, southeast China, northern Iran, and the
589 southern Arabian Sea. The TFA wet deposition was comparable between the two models.
590 • There are large variations in TFA rainwater concentrations associated with rainfall extent. The
591 mean TFA rainwater concentration calculated for the four emission scenarios from GEOS-
592 Chem and WRF-Chem was below the no observable effect concentration (NOEC), suggesting
593 the ecological and human health impacts to be not significant.
594 • With a chemical turnover time of HFO-1234yf of 10 days, its impact is not local and extends
595 well beyond the region of emissions. This study highlights the enhanced TFA formation by the
596 simultaneous use of HFO-1234yf by neighboring regions. If all the Northern Hemisphere
597 countries were to use HFO-1234yf, the impact would be higher by a factor of 2 or 3. However,
598 these amounts are still much lower than the NOEC noted above.
599 • We estimate that continued use of HFO-1234yf in India, China, and the Middle East are
600 unlikely to lead to detrimental human health effects based on the current understanding of the
601 effects of TFA in water bodies, as summarized by Neale et al. (2021). (Note we do not assume
602 the water is treated specifically to remove TFA before consumption.)
603 • We note that a hydrology model of the water flow and TFA concentrations in them would be
604 beneficial to quantify the extent of TFA accumulation in pools and flow out to large water
605 bodies.
606

607 **Acknowledgement:**

608 We are grateful to Jan Kazil (NOAA/CSL) and Rajesh Kumar (NCAR) for help with the WRF-
609 Chem. We are thankful to Jared Brewer and Viral Shah for helping with TFA chemistry in GEOS-
610 Chem. We are thankful to Kirpa Ram for providing the sulfate rainwater concentration data over
611 India. We are grateful to Anwar Khan, Rabi Chhantyal Pun, Dudley Shallcross, and Andrew Orr-
612 Ewing for providing their calculated Criegee intermediate concentrations. This work was funded
613 by the Global Forum for Advanced Climate Technologies.
614

615 **References**

- 616 Amann, M., Bertok, I., Borken-Kleefeld, J., Cofala, J., Heyes, C., Höglund-Isaksson, L.,
617 Klimont, Z., Nguyen, B., Posch, M., Rafaj, P., Sandler, R., Schöpp, W., Wagner, F. and
618 Winiwarter, W.: Cost-effective control of air quality and greenhouse gases in Europe:
619 Modeling and policy applications, *Environ. Model. Softw.*, 26, 1489–1501,
620 doi:10.1016/j.envsoft.2011.07.012, 2011.
621 Amos, H. M., Jacob, D. J., Holmes, C. D., Fisher, J. A., Wang, Q., Yantosca, R. M., Corbitt, E.
622 S., Galarneau, E., Rutter, A. P., Gustin, M. S., Steffen, A., Schauer, J. J., Graydon, J. A., St
623 Louis, V. L., Talbot, R. W., Edgerton, E. S., Zhang, Y. and Sunderland, E. M.: Gas-particle
624 partitioning of atmospheric Hg(II) and its effect on global mercury deposition, *Atmos. Chem.*
625 *Phys.*, 12, 591–603, doi:10.5194/acp-12-591-2012, 2012.
626 Boutonnet, J. C., Bingham, P., Calamari, D., de Rooij, C., Franklin, J., Kawano, T., Libre, J.-M.,
627 McCulloch, A., Malinverno, G., Odom, J. M., Rusch, G. M., Smythe, K., Sobolev, I.,
628 Thompson, R. and Tiedje, J. M.: Environmental Risk Assessment of Trifluoroacetic Acid,
629 *Hum. Ecol. Risk Assess. An Int. J.*, 5, 59–124, doi:10.1080/10807039991289644, 2011.



- 630 Burkholder, J. B., Cox, R. A. and Ravishankara, A. R.: Atmospheric Degradation of Ozone
631 Depleting Substances, Their Substitutes, and Related Species, *Chem. Rev.*, 115, 3704–3759,
632 doi:10.1021/cr5006759, 2015.
- 633 Chen, H., Zhang, L., Li, M., Yao, Y., Zhao, Z., Munoz, G. and Sun, H.: Per- and polyfluoroalkyl
634 substances (PFASs) in precipitation from mainland China: Contributions of unknown
635 precursors and short-chain (C2–C3) perfluoroalkyl carboxylic acids, *Water Res.*, 153, 169–
636 177, doi:10.1016/j.watres.2019.01.019, 2019.
- 637 Chhantyal-Pun, R., McGillen, M. R., Beames, J. M., Khan, M. A. H., Percival, C. J., Shallcross,
638 D. E. and Orr-Ewing, A. J.: Temperature-Dependence of the Rates of Reaction of
639 Trifluoroacetic Acid with Criegee Intermediates, *Angew. Chemie - Int. Ed.*, 56, 9044–9047,
640 doi:10.1002/anie.201703700, 2017.
- 641 David, L. M., Ravishankara, A. R., Kodros, J. K., Venkataraman, C., Sadavarte, P., Pierce, J. R.,
642 Chaliyakunnel, S. and Millet, D. B.: Aerosol Optical Depth Over India, *J. Geophys. Res.*
643 *Atmos.*, 123(7), 1–16, doi:10.1002/2017JD027719, 2018.
- 644 David, L. M., Ravishankara, A. R., Kodros, J. K., Pierce, J. R., Venkataraman, C. and Sadavarte,
645 P.: Premature Mortality Due to PM_{2.5} Over India: Effect of Atmospheric Transport and
646 Anthropogenic Emissions, *GeoHealth*, 3(1), 2–10, doi:10.1029/2018GH000169, 2019.
- 647 Duan, Y., Sun, H., Yao, Y., Meng, Y. and Li, Y.: Distribution of novel and legacy per-
648 /polyfluoroalkyl substances in serum and its associations with two glycemic biomarkers among
649 Chinese adult men and women with normal blood glucose levels, *Environ. Int.*, 134(105295),
650 doi:10.1016/j.envint.2019.105295, 2020.
- 651 Fast, J. D., Gustafson, W. I., Easter, R. C., Zaveri, R. A., Barnard, J. C., Chapman, E. G., Grell,
652 G. A. and Peckham, S. E.: Evolution of ozone, particulates, and aerosol direct radiative forcing
653 in the vicinity of Houston using a fully coupled meteorology-chemistry-aerosol model, *J.*
654 *Geophys. Res. Atmos.*, 111(D21305), 1–29, doi:10.1029/2005JD006721, 2006.
- 655 Fortems-Cheiney, A., Saunois, M., Pison, I., Chevallier, F., Bousquet, P., Cressot, C., Montzka,
656 S. A., Fraser, P. J., Vollmer, M. K., Simmonds, P. G., Young, D., O’Doherty, S., Weiss, R. F.,
657 Artuso, F., Barletta, B., Blake, D. R., Li, S., Lunder, C., Miller, B. R., Park, S., Prinn, R., Saito,
658 T., Steele, L. P. and Yokouchi, Y.: Increase in HFC-134a emissions in response to the success
659 of the Montreal protocol, *J. Geophys. Res.*, 120(22), 11,728–11,742,
660 doi:10.1002/2015JD023741, 2015.
- 661 Freeling, F., Behringer, D., Heydel, F., Scheurer, M., Ternes, T. A. and Nöddler, K.:
662 Trifluoroacetate in Precipitation: Deriving a Benchmark Data Set, *Environ. Sci. Technol.*,
663 54(18), 11210–11219, doi:10.1021/acs.est.0c02910, 2020.
- 664 George, C., Saison, J. Y., Ponche, J. L. and Mirabel, P.: Kinetics of mass transfer of carbonyl
665 fluoride, trifluoroacetyl fluoride, and trifluoroacetyl chloride at the air/water interface, *J. Phys.*
666 *Chem.*, 98(42), 10857–10862, doi:10.1021/j100093a029, 1994.
- 667 Giglio, L., Randerson, J. T. and Van Der Werf, G. R.: Analysis of daily, monthly, and annual
668 burned area using the fourth-generation global fire emissions database (GFED4), *J. Geophys.*
669 *Res. Biogeosciences*, 118(1), 317–328, doi:10.1002/jgrg.20042, 2013.
- 670 Grell, G. A., Knoche, R., Peckham, S. E. and McKeen, S. A.: Online versus offline air quality
671 modeling on cloud-resolving scales, *Geophys. Res. Lett.*, 31(16117),
672 doi:10.1029/2004GL020175, 2004.
- 673 Grell, G. A., Peckham, S. E., Schmitz, R., McKeen, S. A., Frost, G., Skamarock, W. C. and Eder,
674 B.: Fully coupled “online” chemistry within the WRF model, *Atmos. Environ.*, 39, 6957–6975,
675 doi:10.1016/j.atmosenv.2005.04.027, 2005.



- 676 Guenther, A.: Erratum: Estimates of global terrestrial isoprene emissions using MEGAN (Model
677 of Emissions of Gases and Aerosols from Nature) (Atmospheric Chemistry and Physics (2006)
678 6 (3181-3210)), *Atmos. Chem. Phys.*, 7, 4327, doi:10.5194/acp-7-4327-2007, 2007.
- 679 Guenther, A. B., Jiang, X., Heald, C. L., Sakulyanontvittaya, T., Duhl, T., Emmons, L. K. and
680 Wang, X.: The model of emissions of gases and aerosols from nature version 2.1
681 (MEGAN2.1): An extended and updated framework for modeling biogenic emissions, *Geosci.
682 Model Dev.*, 5(6), 1471–1492, doi:10.5194/gmd-5-1471-2012, 2012.
- 683 Henne, S., Shallcross, D. E., Reimann, S., Xiao, P., Brunner, D., O’Doherty, S. and Buchmann,
684 B.: Future emissions and atmospheric fate of HFC-1234yf from mobile air conditioners in
685 Europe, *Environ. Sci. Technol.*, 46, 1650–1658, doi:10.1021/es2034608, 2012.
- 686 Janssens-Maenhout, G., Crippa, M., Guizzardi, D., Dentener, F., Muntean, M., Pouliot, G.,
687 Keating, T., Zhang, Q., Kurokawa, J., Wankmüller, R., Denier Van Der Gon, H., Kuenen, J. J.
688 P., Klimont, Z., Frost, G., Darras, S., Koffi, B. and Li, M.: HTAP-v2.2: A mosaic of regional
689 and global emission grid maps for 2008 and 2010 to study hemispheric transport of air
690 pollution, *Atmos. Chem. Phys.*, 15, 11411–11432, doi:10.5194/acp-15-11411-2015, 2015.
- 691 Kanakidou, M., Dentener, F. J. and Crutzen, P. J.: A global three-dimensional study of the fate of
692 HCFCs and HFC-134a in the troposphere, *J. Geophys. Res. Atmos.*, 100(D9), 18781–18801,
693 1995.
- 694 Kazil, J., McKeen, S., Kim, S. W., Ahmadov, R., Grell, G. A., Talukdar, R. K. and
695 Ravishankara, A. R.: Deposition and rainwater concentrations of trifluoroacetic acid in the
696 United States from the use of hfo-1234yf, *J. Geophys. Res.*, 119, 14,059-14,079,
697 doi:10.1002/2014JD022058, 2014.
- 698 Khan, M. A. H., Percival, C. J., Caravan, R. L., Taatjes, C. A. and Shallcross, D. E.: Criegee
699 intermediates and their impacts on the troposphere, *Environ. Sci. Process. Impacts*, 20, 437–
700 453, doi:10.1039/c7em00585g, 2018.
- 701 Kotamarthi, V. R., Rodriguez, J. M., Ko, M. K. W., Tromp, T. K. and Sze, N. D.: Trifluoroacetic
702 acid from degradation of HCFCs and HFCs: A three-dimensional modeling study, *J. Geophys.
703 Res.*, 103(D5), 5747–5758, 1998.
- 704 Kuhns, H., Knipping, E. and Vukovich, J.: Development of a United States–Mexico emissions
705 inventory for the Big Bend regional aerosol and visibility observational (Bravo) study, *J. Air
706 Waste Manag. Assoc.*, 55(5), 677–692, doi:10.1080/10473289.2005.10464648, 2005.
- 707 Kumar, R., Naja, M., Pfister, G. G., Barth, M. C., Wiedinmyer, C. and Brasseur, G. P.:
708 Simulations over South Asia using the Weather Research and Forecasting model with
709 Chemistry (WRF-Chem): Chemistry evaluation and initial results, *Geosci. Model Dev.*, 5(3),
710 619–648, doi:10.5194/gmd-5-619-2012, 2012.
- 711 Kumar, R., Barth, M. C., Pfister, G. G., Delle Monache, L., Lamarque, J. F., Archer-Nicholls, S.,
712 Tilmes, S., Ghude, S. D., Wiedinmyer, C., Naja, M. and Walters, S.: How Will Air Quality
713 Change in South Asia by 2050?, *J. Geophys. Res. Atmos.*, 123, 1840–1864,
714 doi:10.1002/2017JD027357, 2018a.
- 715 Kumar, S., Kachhawa, S., Goenka, A., Kasamsetty, S. and George, G.: Demand analysis for
716 cooling by sector in India in 2027, New Delhi: Alliance for an Energy Efficient Economy.,
717 2018b.
- 718 Li, M., Zhang, Q., Kurokawa, J. I., Woo, J. H., He, K., Lu, Z., Ohara, T., Song, Y., Streets, D.
719 G., Carmichael, G. R., Cheng, Y., Hong, C., Huo, H., Jiang, X., Kang, S., Liu, F., Su, H. and
720 Zheng, B.: MIX: A mosaic Asian anthropogenic emission inventory under the international
721 collaboration framework of the MICS-Asia and HTAP, *Atmos. Chem. Phys.*, 17(2), 935–963,



- 722 doi:10.5194/acp-17-935-2017, 2017.
- 723 Liu, H., Jacob, D. J., Bey, I. and Yantosca, R. M.: Constraints from ^{210}Pb and ^7Be on wet
724 deposition and transport in a global three-dimensional chemical tracer model driven by
725 assimilated meteorological fields, *J. Geophys. Res. Atmos.*, 106(D11), 12,109-12,128,
726 doi:10.1029/2000JD900839, 2001.
- 727 Luecken, D. J., Waterland, R. L., Papasavva, S., Taddonio, K. N., Hutzell, W. T., Rugh, J. P. and
728 Andersen, S. O.: Ozone and TFA impacts in North America from degradation of 2,3,3,3-
729 tetrafluoropropene (HF0-1234yf), A potential greenhouse gas replacement, *Environ. Sci.*
730 *Technol.*, 44, 343–348, doi:10.1021/es902481f, 2010.
- 731 Myhre, G., Shindell, D., Bréon, F.-M., Collins, W., Fuglestedt, J., Huang, J., Koch, D.,
732 Lamarque, J.-F., Lee, D., Mendoza, B., Nakajima, T., Robock, A., Stephens, G., Takemura, T.
733 and Zhang, H.: Anthropogenic and Natural Radiative Forcing, edited by T. F. Stocker, D. Qin,
734 G.-K. Plattner, M. Tignor, S. K. Allen, J. Boschung, A. Nauels, Y. Xia, V. Bex, and P. M.
735 Midgley, Cambridge University Press, Cambridge, United Kingdom and New York, NY,
736 USA., 2013.
- 737 Neale, R. E., Barnes, P. W., Robson, T. M., Neale, P. J., Williamson, C. E., Zepp, R. G., Wilson,
738 S. R., Madronich, S., Andrady, A. L., Heikkilä, A. M., Bernhard, G. H., Bais, A. F., Aucamp,
739 P. J., Banaszak, A. T., Bornman, J. F., Bruckman, L. S., Byrne, S. N., Foereid, B., Häder, D.-
740 P., Hollestein, L. M., Hou, W.-C., Hylander, S., Jansen, M. A. K., Klekociuk, A. R., Liley, J.
741 B., Longstreth, J., Lucas, R. M., Martinez-Abaigar, J., McNeill, K., Olsen, C. M., Pandey, K.
742 K., Rhodes, L. E., Robinson, S. A., Rose, K. C., Schikowski, T., Solomon, K. R., Sulzberger,
743 B., Ukpebor, J. E., Wang, Q.-W., Wängberg, S.-Å., White, C. C., Yazar, S., Young, A. R.,
744 Young, P. J., Zhu, L. and Zhu, M.: Environmental effects of stratospheric ozone depletion, UV
745 radiation, and interactions with climate change: UNEP Environmental Effects Assessment
746 Panel, Update 2020, *Photochem. Photobiol. Sci.*, doi:10.1007/s43630-020-00001-x, 2021.
- 747 Neu, J. L. and Prather, M. J.: Toward a more physical representation of precipitation scavenging
748 in global chemistry models: Cloud overlap and ice physics and their impact on tropospheric
749 ozone, *Atmos. Chem. Phys.*, 12, 3289–3310, doi:10.5194/acp-12-3289-2012, 2012.
- 750 Pandey, A., Sadavarte, P., Rao, A. B. and Venkataraman, C.: A technology-linked multi-
751 pollutant inventory of Indian energy-use emissions: II. Residential, agricultural and informal
752 industry sectors, *Atmos. Environ.*, 99, 341–352, doi:10.1016/j.atmosenv.2014.09.080, 2014.
- 753 Papadimitriou, V. C., Talukdar, R. K., Portmann, R. W., Ravishankara, A. R. and Burkholder, J.
754 B.: CF₃CF=CH₂ and (Z)-CF₃CF=CHF: Temperature dependent OH rate coefficients and
755 global warming potentials, *Phys. Chem. Chem. Phys.*, 10, 808–820, doi:10.1039/b714382f,
756 2008.
- 757 Papasavva, S., Luecken, D. J., Waterland, R. L., Taddonio, K. N. and Andersen, S. O.: Estimated
758 2017 refrigerant emissions of 2,3,3,3-tetrafluoropropene (HFC-1234yf) in the United States
759 resulting from automobile air conditioning, *Environ. Sci. Technol.*, 43(24), 9252–9259,
760 doi:10.1021/es902124u, 2009.
- 761 Pfister, G. G., Avise, J., Wiedinmyer, C., Edwards, D. P., Emmons, L. K., Diskin, G. D.,
762 Podolske, J. and Wisthaler, A.: CO source contribution analysis for California during
763 ARCTAS-CARB, *Atmos. Chem. Phys.*, 11, 7515–7532, doi:10.5194/acp-11-7515-2011, 2011.
- 764 Purohit, P. and Höglund-Isaksson, L.: Global emissions of fluorinated greenhouse gases 2005-
765 2050 with abatement potentials and costs, *Atmos. Chem. Phys.*, 17, 2795–2816,
766 doi:10.5194/acp-17-2795-2017, 2017.
- 767 Purohit, P., Höglund-Isaksson, L., Dulac, J., Shah, N., Wei, M., Rafaj, P. and Schöpp, W.:



- 768 Electricity savings and greenhouse gas emission reductions from global phase-down of
769 hydrofluorocarbons, *Atmos. Chem. Phys.*, 20, 11305–11327, doi:10.5194/acp-20-11305-2020,
770 2020.
- 771 Rigby, M., Montzka, S. A., Prinn, R. G., White, J. W. C., Young, D., O’Doherty, S., Lunt, M. F.,
772 Ganesan, A. L., Manning, A. J., Simmonds, P. G., Salameh, P. K., Harth, C. M., Mühle, J.,
773 Weiss, R. F., Fraser, P. J., Steele, L. P., Krummel, P. B., McCulloch, A. and Park, S.: Role of
774 atmospheric oxidation in recent methane growth, *Proc. Natl. Acad. Sci. U. S. A.*, 114(21),
775 5373–5377, doi:10.1073/pnas.1616426114, 2017.
- 776 Russell, M. H., Hoogeweg, G., Webster, E. M., Ellis, D. A., Waterland, R. L. and Hoke, R. A.:
777 TFA from HFO-1234yf: Accumulation and aquatic risk in terminal water bodies, *Environ.*
778 *Toxicol. Chem.*, 31(9), 1957–1965, doi:10.1002/etc.1925, 2012.
- 779 Sadavarte, P. and Venkataraman, C.: Trends in multi-pollutant emissions from a technology-
780 linked inventory for India: I. Industry and transport sectors, *Atmos. Environ.*, 99, 353–364,
781 doi:10.1016/j.atmosenv.2014.09.081, 2014.
- 782 Solomon, K. R., Velders, G. J. M., Wilson, S. R., Madronich, S., Longstreth, J., Aucamp, P. J.
783 and Bornman, J. F.: Sources, fates, toxicity, and risks of trifluoroacetic acid and its salts:
784 Relevance to substances regulated under the Montreal and Kyoto Protocols, *J. Toxicol.*
785 *Environ. Heal. Part B*, 19(7), 289–304, doi:10.1080/10937404.2016.1175981, 2016.
- 786 Tilmes, S., Lamarque, J. F., Emmons, L. K., Kinnison, D. E., Ma, P. L., Liu, X., Ghan, S.,
787 Bardeen, C., Arnold, S., Deeter, M., Vitt, F., Ryerson, T., Elkins, J. W., Moore, F., Spackman,
788 J. R. and Val Martin, M.: Description and evaluation of tropospheric chemistry and aerosols in
789 the Community Earth System Model (CESM1.2), *Geosci. Model Dev.*, 8, 1395–1426,
790 doi:10.5194/gmd-8-1395-2015, 2015.
- 791 Velders, G. J. M., Fahey, D. W., Daniel, J. S., McFarland, M. and Andersen, S. O.: The large
792 contribution of projected HFC emissions to future climate forcing, *Proc. Natl. Acad. Sci. U. S.*
793 *A.*, 106(27), 10949–10954, doi:10.1073/pnas.0902817106, 2009.
- 794 Velders, G. J. M., Fahey, D. W., Daniel, J. S., Andersen, S. O. and McFarland, M.: Future
795 atmospheric abundances and climate forcings from scenarios of global and regional
796 hydrofluorocarbon (HFC) emissions, *Atmos. Environ.*, 123, 200–209,
797 doi:10.1016/j.atmosenv.2015.10.071, 2015.
- 798 Wang, Z., Wang, Y., Li, J., Henne, S., Zhang, B., Hu, J. and Zhang, J.: Impacts of the
799 Degradation of 2,3,3,3-Tetrafluoropropene into Trifluoroacetic Acid from Its Application in
800 Automobile Air Conditioners in China, the United States, and Europe, *Environ. Sci. Technol.*,
801 52, 2819–2826, doi:10.1021/acs.est.7b05960, 2018.
- 802 Wesely, M. L.: Parameterization of Surface Resistances to Gaseous Dry Deposition in Regional-
803 Scale Numerical Models, *Atmos. Environ.*, 23(6), 1293–1304, doi:10.1016/S0950-
804 351X(05)80241-1, 1989.
- 805 Wiedinmyer, C., Akagi, S. K., Yokelson, R. J., Emmons, L. K., Al-Saadi, J. A., Orlando, J. J.
806 and Soja, A. J.: The Fire INventory from NCAR (FINN): A high resolution global model to
807 estimate the emissions from open burning, *Geosci. Model Dev.*, 4, 625–641, doi:10.5194/gmd-
808 4-625-2011, 2011.
- 809 World Meteorological Organization: Scientific Assessment of Ozone Depletion: 2006; WMO:
810 Geneva, Switzerland, , 50, 572, 2007.
- 811 Young, C. J. and Mabury, S. A.: Atmospheric Perfluorinated Acid Precursors: Chemistry,
812 Occurrence, and Impacts, *Rev. Environ. Contam. Toxicol.* Vol. 208, 1–109, 2010.
- 813



814 **Tables**

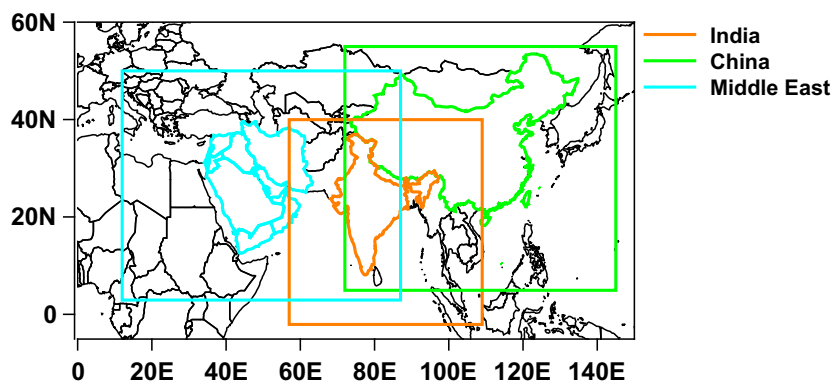
815 **Table 1.** The slope, correlation coefficient (R), intercept (c), mean bias (MB), and the number of
816 points (N) of simulated (GEOS-Chem) and observed sulfate rainwater concentration over the three
817 domains.

Region	Slope	R	c	MB	N
India	0.771	0.816	0.210	-0.255±0.778	54
China	0.799	0.911	0.655	-1.07±2.700	89
Middle East	1.42	0.880	-2.81	-0.187±2.71	5

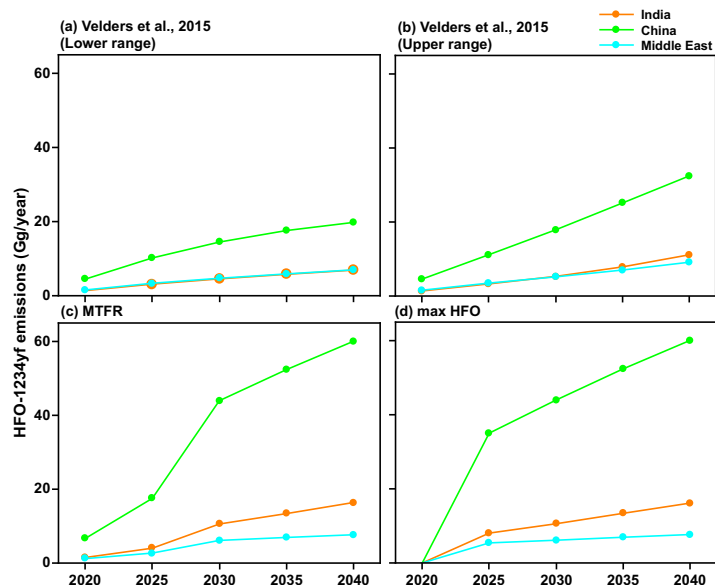
818



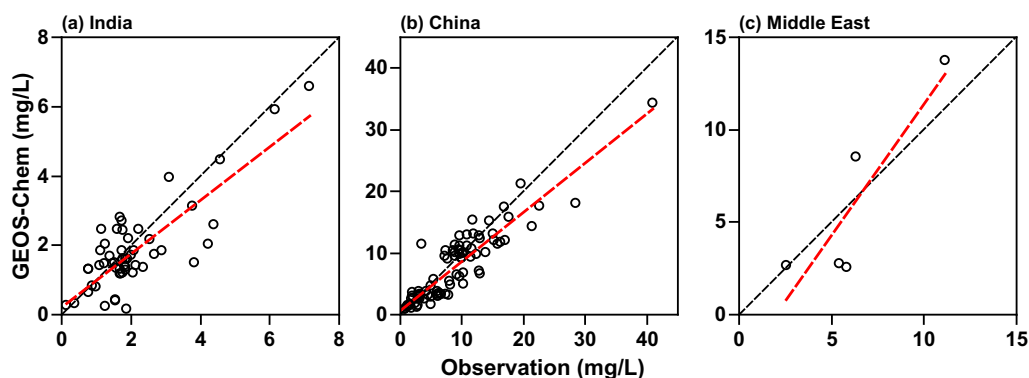
819 **Figures**



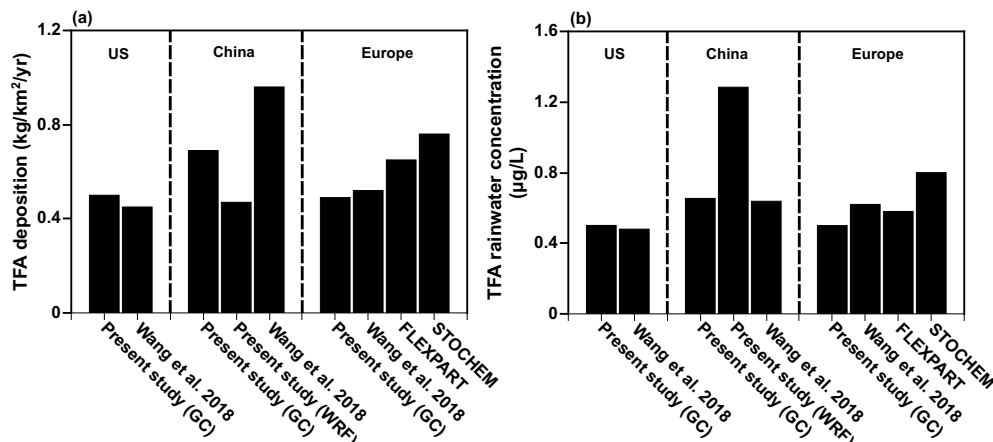
820
821 **Figure 1.** The model domains for India, China, and the Middle East used in the present study and
822 also for WRF-Chem simulations. The land regions for the emissions are shown in color.
823
824



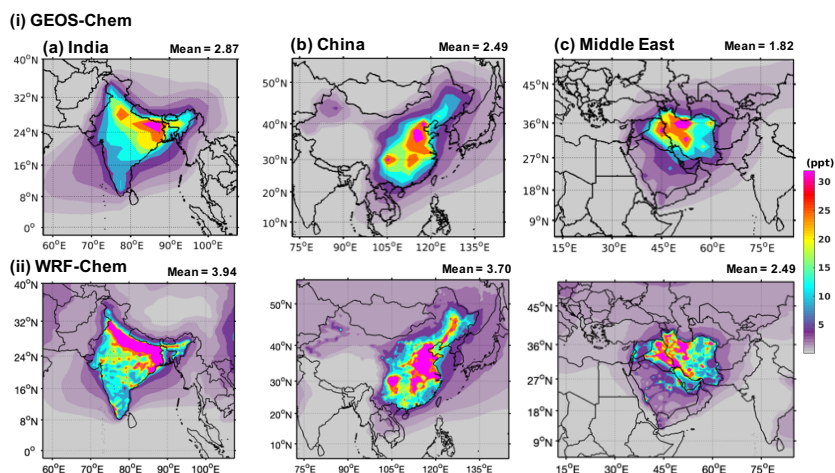
825
826 **Figure 2.** The projected HFO-1234yf emissions scenarios between 2020 and 2040 from Velders
827 et al. (2015) (a) lower and (b) upper ranges, IIASA GAINS model for (c) Maximum Technically
828 Feasible Reduction (MTFR) and (d) max HFO in India, China, and the Middle East.
829



830
831 **Figure 3.** Scatter plot of simulated and observed sulfate rainwater concentration in (a) India, (b)
832 China, and (c) the Middle East for 2000-2015. The linear regression line is shown in red. The black
833 dashed line corresponds to slope = 1. The data for the Middle East are very limited.
834
835

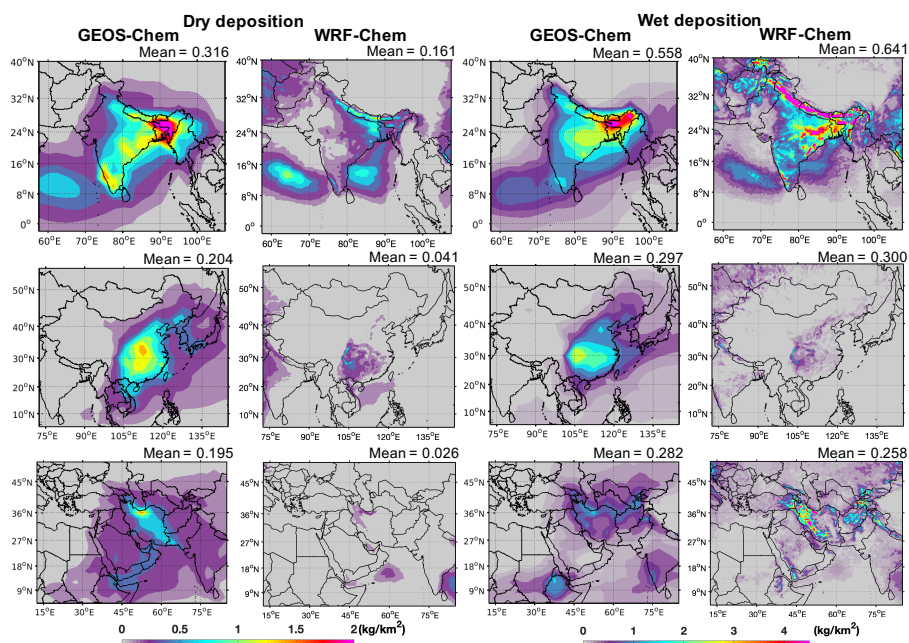


836
837 **Figure 4.** Comparison of the present study with other studies over the U.S., China, and Europe for
838 (a) TFA deposition, and (b) TFA rainwater concentration. Note the emissions are 24.53 Gg yr⁻¹,
839 42.65 Gg yr⁻¹, and 19.16 Gg yr⁻¹ for the U.S., China, and Europe, respectively.
840



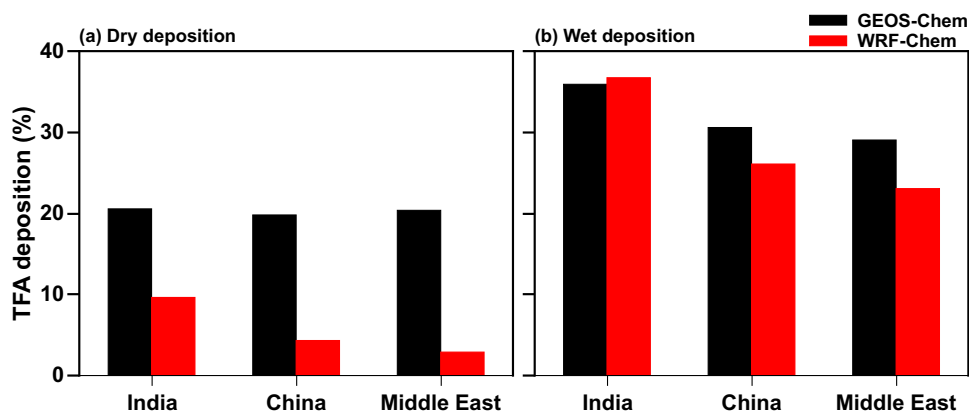
841
 842
 843
 844
 845
 846

Figure 5. Annual mean surface mixing ratios of HFO-1234yf simulated in (i) GEOS-Chem and (ii) WRF-Chem over (a) India, (b) China, and (c) the Middle East. The number at the top of each panel gives the mean HFO-1234yf mixing ratios within the domains.



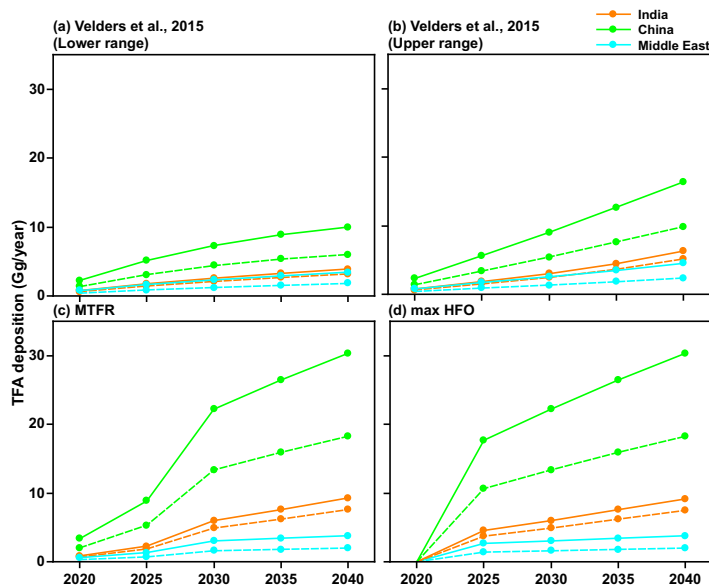
847
 848
 849
 850
 851

Figure 6. GEOS-Chem and WRF-Chem simulated annual total deposition rates of TFA ($\text{kg km}^{-2} \text{yr}^{-1}$) from (a) dry and (b) wet deposition in India, China, and the Middle East domains. The number at the top of each panel gives the mean dry and wet deposition rates within the domains.



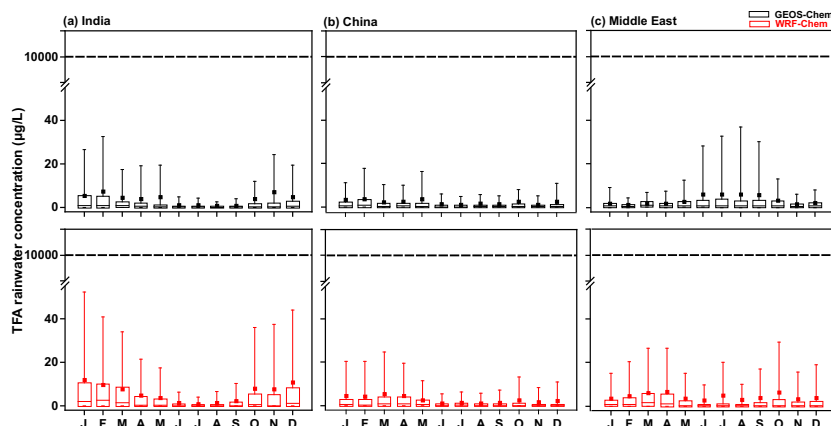
852
853
854
855
856

Figure 7. Percentage contribution of (a) dry and (b) wet deposition to total annual TFA deposition simulated in GEOS-Chem and WRF-Chem in the three domains.



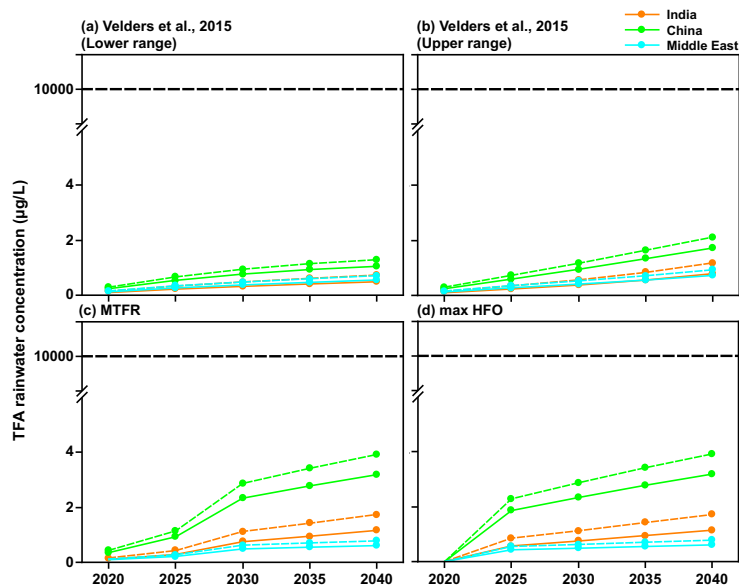
857
858
859
860
861
862

Figure 8. Total TFA deposited (dry and wet combined) in four emission scenarios for 2020 to 2040 within India, China, and the Middle East domains calculated using GEOS-Chem (solid lines) and WRF-Chem (dashed lines). The values from the two models are reasonably close for India and the Middle East, while they differ by almost a factor two for China.



863
 864
 865
 866
 867
 868
 869
 870
 871
 872

Figure 9. Box and whisker plot of TFA rainwater concentration calculated from GEOS-Chem and WRF-Chem in the three domains. In the box plot, the inside line and square are the median and mean, respectively. Box boundaries are 25th and 75th percentiles, and whiskers indicate the 5th and 95th percentiles. The dashed horizontal line is the No Observable Effect Concentration (NOEC) level. It is important to note that these values, including the 95th percentile values are at least 100 times lower than the NOEC for harming aquatic bodies even when normalized for higher projected emissions in 2040.

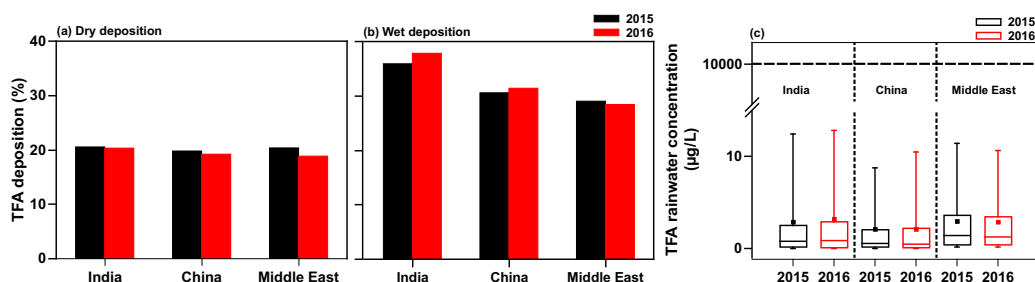


873
 874
 875
 876
 877

Figure 10. Mean TFA rainwater concentration in four scenarios for 2020 to 2040 for India, China, and the Middle East domains calculated using GEOS-Chem (solid lines) and WRF-Chem (dashed lines). The NOEC is denoted above, and it is two orders of magnitude larger than calculated TFA concentrations for any of the scenarios.



878

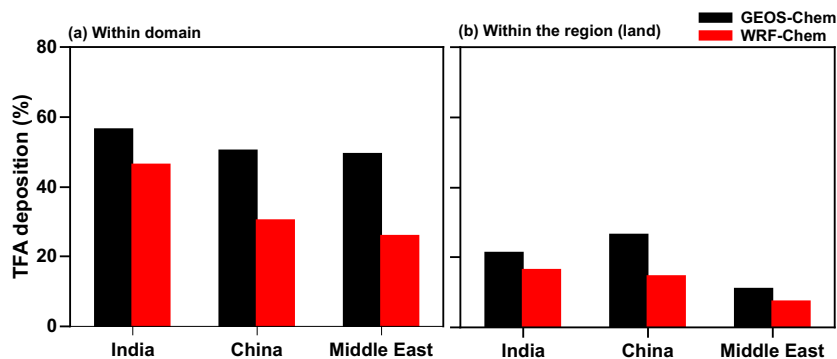


879

880 **Figure 11.** Annual percentage of total TFA (a) dry and (b) wet deposition, and (c) annual mean
881 TFA rainwater concentrations in India, China, and the Middle East domains from GEOS-Chem
882 for 2015 and 2016. The dashed horizontal line is the NOEC level.

883

884

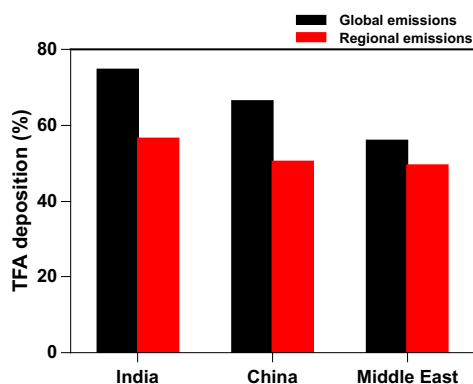


885

886 **Figure 12.** Annual percentage of total TFA deposition (dry and wet combined) calculated from
887 GEOS-Chem and WRF-Chem within the three (a) domains and (b) regions (land).

888

889

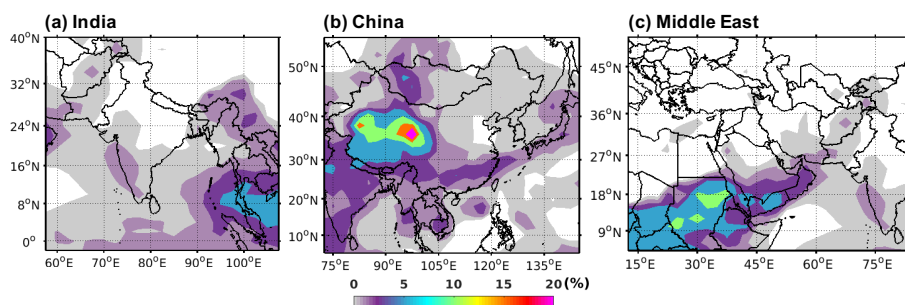


890

891 **Figure 13.** Annual percentage of total TFA deposition (dry and wet combined) in India, China,
892 and the Middle East from global and regional (individual regions) emissions.



893



894

895 **Figure 14.** Percentage decrease in TFA deposition (dry and wet combined) by adding Criegee
896 intermediate chemistry in (a) India, (b) China, and (c) the Middle East domains.

897